The Astrophysical Journal, 779:119 (11pp), 2013 December 20 doi:10.1088/0004-637X/779/2/119

THE FIRST ASTROPHYSICAL DETECTION, TERAHERTZ SPECTRUM, AND DATABASE FOR THE MONODEUTERATED SPECIES OF METHYL FORMATE $HCOOCH_2D$

L. H. Coudert[1], B. J. Drouin[2], B. Tercero[3], J. Cernicharo[3], J.-C. Guillemin[4], R. A. Motiyenko[5], and L. Margulès[5]
[1] LISA, UMR 7583 CNRS-Universités Paris Est Créteil et Paris Diderot, 61 Avenue du Général de Gaulle, F-94010 Créteil, France; laurent.coudert@lisa.u-pec.fr
[2] Jet Propulsion Laboratory, California Institute of Technology, Pasadena, CA 91109, USA
[3] Centro de Astrobiologia (CSIC-INTA), Laboratory of Molecular Astrophysics, Department of Astrophysics, Ctra de Ajalvir, Km 4, E-28850 Torrejón de Ardoz, Madrid, Spain
[4] Institut des Sciences Chimiques de Rennes, UMR 6226 CNRS-ENSCR, 11 Allée de Beaulieu, CS 50837, F-35708 Rennes Cedex 7, France
[5] Laboratoire de Physique des Lasers, Atomes et Molécules, UMR 8523 CNRS-Université Lille I, Bât. P5, F-59655 Villeneuve d'Ascq Cedex, France
Received 2013 July 10; accepted 2013 October 13; published 2013 December 2

ABSTRACT

Based on new measurements carried out in the laboratory from 0.77 to 1.2 THz and on a line-frequency analysis of these new data, along with previously published data, we build a line list for $HCOOCH_2D$ that leads to its first detection in the Orion KL nebula. The observed lines, both in space and in the laboratory, involve the *cis* D-in-plane and *trans* D-out-of-plane conformations of $HCOOCH_2D$ and the two tunneling states arising from the large-amplitude motion connecting the two *trans* configurations. The model used in the line position calculation accounts for both *cis* and *trans* conformations, as well as the large-amplitude motion.

Key words: astronomical databases: miscellaneous – ISM: individual objects (Orion KL) – ISM: molecules – line: identification – methods: data analysis – methods: laboratory: molecular – submillimeter: ISM

Online-only material: color figures, machine-readable tables

1. INTRODUCTION

Methyl formate ($HCOOCH_3$) is a non-rigid complex organic molecule of astrophysical relevance displaying a rich microwave spectrum that has been the subject of extensive laboratory studies (Curl 1959; Brown et al. 1975; Bauder 1979; Demaison et al. 1983; Plummer et al. 1984, 1986; Oesterling et al. 1999; Karakawa et al. 2001; Ogata et al. 2004; Carvajal et al. 2007; Ilyushin et al. 2009; Demaison et al. 2010; Tudorie et al. 2011). The normal species of methyl formate was first detected as early as 1975 by Brown et al. (1975) in Sgr B2. It was later detected in the hot cores of giant molecular clouds, in star-forming regions, and in comets (Blake et al. 1986; Nummelin et al. 2000; Kobayashi et al. 2007; Demyk et al. 2008). Due to the importance of deuterium fractionation (Herbst 1992), detections of its monodeuterated isotopic variants have also been attempted. The monodeuterated species $DCOOCH_3$, with a deuterated carbonyl group, has been tentatively detected in Orion (Margulès et al. 2010) and in the protostar IRAS 16293-2422 (Demyk et al. 2010). However, no attempt has been made to detect the monodeuterated species $HCOOCH_2D$, with a deuterated methyl group, although its microwave spectrum has already been investigated (Margulès et al. 2009a).

In this paper, following the strategy of our previous papers devoted to methyl formate (Carvajal et al. 2009; Margulès et al. 2010; Tercero et al. 2012), we report the first detection of the monodeuterated species $HCOOCH_2D$ in space by means of 66 unblended lines found in the Orion KL nebula's line survey performed with the IRAM 30 m telescope (Tercero et al. 2010, 2011). In this paper, we also build an astrophysical database for this isotopic species that is computed using the results of a line-frequency analysis of new terahertz transitions, recorded in the present investigation in the 0.77–1.2 THz region, along with previously published submillimeter-wave transitions (Margulès et al. 2009a). The database is formatted like the catalog line files of the Jet Propulsion Laboratory (JPL) and, thanks to the extended frequency range of the new dataset, spans the 50 GHz to 1.2 THz region.

2. DATASETS AND LINE ASSIGNMENTS

The laboratory spectra measured in this work were recorded using the Frequency Multiplied Submillimeter Spectrometer (FMSS; Drouin et al. 2005) at JPL. The FMSS was scanned through the 0.77–0.85 THz and 0.95–1.2 THz ranges with three separate multiplier chains. The sample of deuterated methyl formate, previously used by Margulès et al. (2009a), was shipped to JPL and transferred into a sealed 10 cm diameter, 3 m length quartz tube for scans at pressures of 30 mTorr, except for the last scan, from 0.95 to 1.06 THz, which was scanned with a lower pressure of 8 mTorr due to a limited amount of sample. Spectra were recorded with a fine step size of 108–144 kHz and detected in direct absorption using a Schottky diode detector built by Virgina Diodes (WR1.2 ZBD). The voltage rectified at the diode detector was amplified immediately with an Analog Modules pre-amplifier (321A-2-4.7-NI) with a 1.4 kΩ input impedance. Following the pre-amplification, the frequency-modulated source signal was demodulated at twice the modulation rate for a second harmonic detection of the absorption with reduced background fluctuations. Nearly identical conditions were utilized for similar isotopic scans of ^{13}C substituted methyl formate and the other deuterated form of methyl formate ($DCOOCH_3$). The raw spectra are archived at JPL and are available upon request to the authors.

The center frequencies of the isolated and blended features were measured from the raw spectra such as the single spectrum shown in Figure 1, which shows a portion of the spectrum recorded at JPL in the 840000–840400 MHz frequency range. The highest frequency sweep, from 1.06 to 1.20 THz, is shown in Figure 2. That the large features are cut off of the intensity scale is due to partially and fully deuterated water, which appears as an impurity in all scans. The source power, as well as atmospheric absorption near 1.10, 1.11, 1.53, and 1.63 THz, produce the broad variations in the signal across the band, which has roughly equal intensity strong lines in every 1 GHz segment. The line density decreases with increasing frequency, with 20 lines GHz^{-1} detected in

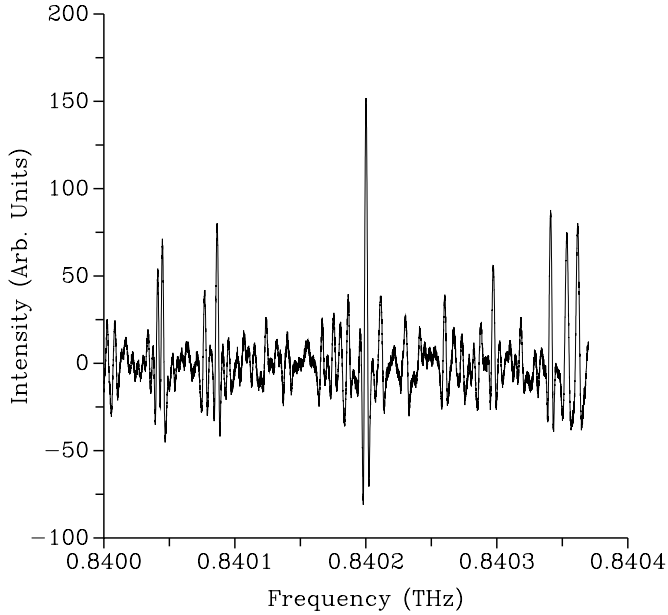

Figure 1. Portion of the spectrum recorded using the JPL experimental setup. The experimental line at 0.8402 THz is a singlet line belonging to the D-in-plane conformation. The two experimental lines at 0.84035 and 0.84036 THz belong to CH_2DOH.

this (highest frequency) sweep. However, the asymmetric-top patterns are all intermixed with only the mid-K ranges of b-type branches readily detected. With little pattern recognition available, the broadband coverage and the slowly varying source power enable confident assignments and permit some ability to judge the character of potentially blended features. Assigned lines were given a 100 kHz uncertainty. Strong isolated lines are significantly more accurate, but the spectrum is dominated by overlapping lines.

The $HCOOCH_2D$ species of methyl formate displays two conformations that are a few cm^{-1} apart. The lower lying one corresponds to the D-in-plane configuration and the upper lying one corresponds to the two energetically equivalent D-out-of-plane configurations (Coudert et al. 2012, Figure 3). Both conformations give rise to a- and b-type transitions. Due to the internal rotation motion taking place for the D-out-of-plane conformation, transitions within this conformation are split into two tunneling components and weak c-type transitions between the two tunneling sublevels can also be observed (Margulès et al. 2009a).

Table 1
Number of Assigned Transitions[a] for Each Conformation and for Each Dataset

Dataset	D-in-plane	D-out-of-plane	Both Conformations
Margulès et al. (2009a)	433	739	1172
This work	765	885	1650
All	1198	1624	2822

Note. [a] The number of lines assigned in the experimental spectra is given. The actual number of lines is larger as both datasets include unresolved multiplets.

The assignment of the transitions measured at JPL was initiated using predictions based on the results of Margulès et al. (2009a) and strong a-type transitions could be identified. Using a bootstrap approach, a preliminary line frequency analysis was carried out and new transitions were predicted and searched for. This procedure was repeated and allowed us to also assign all a-type transitions. Afterward, b-type transitions were then assigned for both conformations. The total number of assigned experimental lines is 2822 and corresponds to 5279 transitions as many lines are unresolved multiplets depending on whether the K-type and/or the tunneling splittings were resolved. Table 1 gives the number of assigned lines for each conformation. In the present dataset, the maximum J- and K_a-values are 84 and 41, respectively. The assigned lines include 1466, 1321, and 28 a-, b-, and c-type transitions, respectively. About seven rotation-tunneling transitions with $\Delta K_a = \Delta K_c = 0$, which are allowed by symmetry, were also measured.

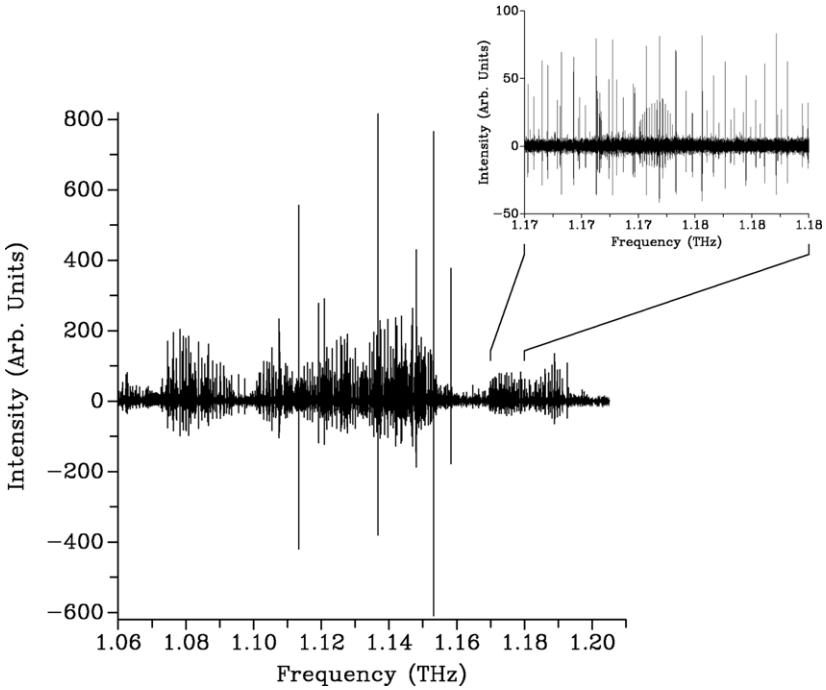

Figure 2. Spectrum recorded between 1.06 and 1.20 THz; the inset shows detail including an unidentified band that is likely to belong to an excited vibrational state of deuterated methyl formate.

Table 2
Assignments[a], Observed Frequencies[b], and Observed Minus Calculated Differences[c] in the Microwave Spectrum[d] of $HCOOCH_2D$

J'	K'_a	K'_c	±	J''	K''_a	K''_c	±	Obs.	Diff.	Multiplet	Ref.
24	18	6		23	17	7		770424.549(100)	−1	*D*	This work
34	14	20		33	13	21		770446.590(100)	37	*D*	This work
63	16	48	+	62	16	47	+	770452.291(100)	8	*D*	This work
76	1	75		75	1	74		770621.252(100)	12	*Q*	This work
30	17	13	+	29	16	14	+	770922.224(100)	20	*Q*	This work
66	16	50		65	16	49		771016.995(100)	2		This work
29	16	13		28	15	14		771059.780(100)	22	*D*	This work
64	13	51		63	13	50		771122.780(100)	−125		This work
67	23	44		66	23	43		771199.377(100)	−331	*D*	This work
72	3	69	+	71	3	68	+	771287.711(100)	−40	*Q*	This work

Notes.
[a] Transitions are assigned with the usual rotational quantum numbers of the upper and lower levels. For transitions of the D-out-of-plane conformation, the + or − signs identify tunneling sublevels. Only the 10 lowest frequency transitions measured in this work appear.
[b] Observed frequency in MHz is given in the column titled "Obs." Experimental uncertainties are given in parentheses in kHz.
[c] Observed minus calculated residuals in kHz are given in the column titled "Diff."
[d] A blank space or the letters *D*, *T*, or *Q*, in the column titled "Multiplet" indicate that the line is a singlet, a doublet, a triplet, or a quadruplet, respectively. The reference to which the line belongs to is given in the column titled "Ref."

(This table is available in its entirety in a machine-readable form in the online journal. A portion is shown here for guidance regarding its form and content.)

3. LINE-FREQUENCY ANALYSIS

The microwave data were analyzed calculating the tunneling-rotational energy with the theoretical approach accounting for the large-amplitude torsional motion proposed by Margulès et al. (2009a). Experimental frequencies were introduced in a least-squares fit procedure where they were given a weight equal to the inverse of the square of their experimental uncertainty. Unresolved multiplets were treated taking for their calculated frequency the average of the calculated frequency of all members of the multiplet.

For the 2822 fitted lines, the root mean square (rms) value of the observed minus calculated residual is 0.16 MHz and the unitless standard deviation is 1.6. For the 1198 (1624) transitions corresponding to the D-in-plane (D-out-of-plane) conformation, the rms value is 0.112 MHz (0.191 MHz). Table 2 lists assignments, observed frequencies, and observed minus calculated differences. Tables 3 and 4 give the values and the uncertainties of the parameters determined in the analysis for the D-in-plane and D-out-of-plane conformations, respectively.

Table 3
Spectroscopic Parameters[a] for the D-in-plane Conformation

Parameter	Value	Parameter	Value
A	19921.587 052(980)	$H_{KJJ} \times 10^9$	20.859(480)
B	6415.266 933(180)	$H_{JJJ} \times 10^9$	2.127(7)
C	5004.268 277(200)	$h_{KK} \times 10^9$	269.470(4797)
		$h_{KJ} \times 10^9$	79.308(600)
$\Delta_{KK} \times 10^3$	77.885 125(4400)	$h_{JJ} \times 10^9$	1.309(3)
$\Delta_{KJ} \times 10^3$	−19.418 282(1000)		
$\Delta_{JJ} \times 10^3$	4.926 657(66)	$L_{KKKK} \times 10^{12}$	−57.549(4797)
$\delta_K \times 10^3$	3.543 944(1900)	$L_{KKKJ} \times 10^{12}$	39.543(1019)
$\delta_J \times 10^3$	1.481 254(26)	$L_{KKJJ} \times 10^{12}$	−10.698(291)
		$L_{KJJJ} \times 10^{12}$	−1.919(30)
$H_{KKK} \times 10^9$	1734.492(8094)	$l_{KJJ} \times 10^{12}$	0.686(57)
$H_{KKJ} \times 10^9$	−714.476(2129)		

Note. [a] Parameters are in MHz. The numbers in parentheses are one standard deviation in the same units as the last digit. These parameters are involved in the pure rotational Hamiltonian in Equation (10) of Margulès et al. (2009a).

4. THE DATABASE

Line strengths were calculated using the values for the dipole moment components listed in Table 5, retrieved from those of the normal species (Margulès et al. 2010). The partition function $Q_{\rm rot}$ was computed for several temperatures taking the degeneracy factors to be equal to $(2J + 1)$. The energy of the 0_{00} level of the D-in-plane conformation was taken to be equal to zero and that of the 0_{00}, + level of the D-out-of-plane conformation was set to 10 cm^{-1}, in agreement with Coudert et al. (2012). Table 6 gives the values thus obtained for the partition functions.

The line list was built calculating the frequencies of the allowed transitions characterized by a rotational quantum number J smaller than 80. Integrated intensities were calculated in $nm^2 \cdot$ MHz units at 300 K using the results given in Tables 5 and 6. Just as in the JPL database (Pickett et al. 1998) catalog line files, the selected transitions are those with an intensity in $nm^2 \cdot$ MHz units at 300 K larger than

$$10^{\rm LOGSTR0} + (F/300,000)^2 \times 10^{\rm LOGSTR1}, \quad (1)$$

where F is the frequency in MHz and LOGSTR0 and LOGSTR1 are two dimensionless constants set to −9 and −7, respectively. The line list, given in Table 7, is formatted in the same way as the catalog line files of the JPL database (Pickett et al. 1998) and gives the line frequency in MHz and the error in MHz, retrieved from the line frequency analysis results, and the base 10 logarithm of the line intensity in $nm^2 \cdot$ MHz at 300 K. Also given are the degrees of freedom of the rotational partition function, the lower state energy in cm^{-1}, the upper state degeneracy, and the species tag and format number. The assignment of the transition is given in the remaining columns in terms of J, K_a, K_c, and the tunneling label. When the calculated error was smaller than 10 kHz, it was set to that value. For observed unblended

Table 4
Spectroscopic Parameters[a] for the D-out-of-plane Conformation

Parameter	Value	Parameter	Value
θ_2	4.796 110(3000)	$f_{2kkk} \times 10^{12}$	49.753(2009)
ϕ_2	85.248 000(5700)	$f_{2kkj} \times 10^{12}$	−13.810(779)
		$f_{2kjj} \times 10^{12}$	−0.512(96)
h_2	−42.837 517(77000)		
		A	18516.681 258(830)
$h_{2k} \times 10^6$	22572.466(1199170)	B	6730.195 643(190)
$h_{2j} \times 10^6$	−1565.485(236836)	C	5164.955 356(180)
$f_2 \times 10^6$	499.174(80944)		
$s_{2xz} \times 10^6$	−6270.914(164886)	$\Delta_{KK} \times 10^3$	57.893 618(2000)
		$\Delta_{KJ} \times 10^3$	−14.761 884(1000)
$h_{2kk} \times 10^6$	−107.451(8094)	$\Delta_{JJ} \times 10^3$	6.207 069(120)
$h_{2kj} \times 10^6$	15.664(2428)	$\delta_K \times 10^3$	1.572 356(2500)
$h_{2jj} \times 10^6$	−1.771(246)	$\delta_J \times 10^3$	1.968 600(66)
$f_{2k} \times 10^6$	−11.012(1289)		
$f_{2j} \times 10^6$	0.461(66)	$H_{KKK} \times 10^9$	821.395(2338)
		$H_{KKJ} \times 10^9$	−9.303(3897)
$h_{2kkk} \times 10^9$	306.733(18287)	$H_{KJJ} \times 10^9$	−69.780(1109)
$h_{2kkj} \times 10^9$	13.391(8394)	$H_{JJJ} \times 10^9$	−3.541(42)
$h_{2kjj} \times 10^9$	−9.135(989)	$h_{KK} \times 10^9$	87.160(11692)
$h_{2jjj} \times 10^9$	0.533(75)	$h_{KJ} \times 10^9$	140.310(899)
$f_{2kk} \times 10^{12}$	−18669.944(3597509)	$h_{JJ} \times 10^9$	−1.601(21)
$f_{2kj} \times 10^{12}$	8445.556(659543)		
$f_{2jj} \times 10^{12}$	−84.167(11092)	$L_{KKJJ} \times 10^{12}$	−6.053(450)
		$L_{KJJJ} \times 10^{12}$	−0.370(147)
$h_{2kkkk} \times 10^{12}$	−160.823(12591)	$L_{JJJJ} \times 10^{12}$	−0.175(4)
$h_{2kkkj} \times 10^{12}$	−54.501(5396)	$l_{KKK} \times 10^{12}$	54.829(2608)
$h_{2kkjj} \times 10^{12}$	19.125(1319)	$l_{KKJ} \times 10^{12}$	77.674(1589)
$h_{2kjjj} \times 10^{12}$	0.349(168)	$l_{KJJ} \times 10^{12}$	5.828(87)
$h_{2jjjj} \times 10^{12}$	−0.046(7)	$l_{JJJ} \times 10^{12}$	−0.079(2)

Note. [a] Parameters are in MHz except θ_2 and ϕ_2, which are in degrees. Numbers in parentheses are one standard deviation in the same units as the last digit. Parameters are defined in Equations (12), (13), and (22) of Margulès et al. (2009a) or are involved in the pure rotational Hamiltonian in Equation (10) of the same reference.

microwave lines, the line frequency and the error were replaced by their experimental values. This is indicated by a negative species tag.

5. DETECTION OF $HCOOCH_2D$ IN ORION KL

We report the first detection of $HCOOCH_2D$ in space by means of 66 unblended lines. The lines of the D-in-plane and the D-out-of-plane configurations were searched for in the Orion KL's line survey performed with the IRAM 30 m telescope (Tercero et al. 2010, 2011).

5.1. Observations and Overall Results

Five observing sessions (two in 2004 September, two in 2005 April, and the last one in 2007 January) have been used to complete the line survey toward the Orion KL nebula in all the frequency ranges available with the IRAM 30 m telescope. The 3.0, 2.0, and 1.3 mm windows (80–115.5 GHz, 130–178 GHz, and 197–281 GHz, respectively) were observed with 1 MHz of spectral resolution. System temperatures were in the range 100–800 K from the lowest to the highest frequencies. We reached the line confusion limit at 1.3 mm where the line density in Orion is extremely high. The spectra were calibrated in antenna temperature using the atmospheric transmission model package (Cernicharo 1985; Pardo et al. 2001). All the observations were performed using the Wobbler Switching mode. The 30 m beam size at the observing frequency ranges from 29″ to 9″ from 80 GHz to 280 GHz. Pointing and focus were checked every 1–2 hr on nearby pointing sources. We pointed toward Orion-IRc2 at $\alpha_{2000.0} = 5^h35^m14^s.5$, $\delta_{2000.0} = -5°22'30''.0$. All frequency settings were repeated at a slightly shifted frequency (10–20 MHz; new tuning was not necessary) in order to remove all possible contributions coming from the image side band. After processing of the data, at least all features in our survey above a 0.05 K threshold are coming from the signals in band. (For a detailed explanation of the observations and data analysis, see Tercero et al. 2010).

During the interpretation of the line survey, we had to deal with more than 15000 spectral features, of which 3600 are still unidentified. Thanks to the close collaboration between spectroscopists and astronomers, around 4400 of these lines have been successfully assigned to several isotopologues of CH_3CH_2CN, CH_2CHCN, $HCOOCH_3$, their vibrational levels and those of abundant molecules (NH_2CHO), and to the recently detected molecules methyl acetate (CH_3COOCH_3) and the gauche conformer of ethyl formate (G-CH_3CH_2OCOH) in this source (Demyk et al. 2007; Carvajal et al. 2009; Margulès et al. 2009b, 2010; Motiyenko et al. 2012; Tercero et al. 2012, 2013; Daly et al. 2013; A. López et al. 2013, in preparation; Haykal et al. 2013a). We also provided tentative detections (phenol c-C_6H_5OH, Kolesniková et al. 2013) and/or upper limit calculations for the column density of non-detected species (allyl-isocyanide CH_2CHCH_2NC, Haykal et al. 2013b). In a parallel work, the study of the survey was divided in the analysis of different families of molecules; this way, we have consistently analyzed these groups of molecules: CS-bearing species (Tercero et al. 2010), silicon-bearing molecules (Tercero et al. 2011), SO and SO_2 (Esplugues et al. 2013a), methyl cyanide (Bell et al. 2013), ethyl cyanide (Daly et al. 2013), HCN, HNC, and HCO^+ (N. Marcelino et al. 2013, in preparation), HC_3N and HC_5N (Esplugues et al. 2013b), and vinyl cyanide (A. López et al. 2013, in preparation). Nevertheless, the analysis of this survey is still open and several works are in progress.

5.2. Results and Astronomical Modeling

Figure 3 shows selected lines from the D-in-plane and D-out-of-plane conformations of $HCOOCH_2D$ present in our Orion data, together with our best model (explained below). All depicted lines are mostly free of blending with other species and in all boxes we observe a significant contribution from the studied species. No unblended lines of either conformation are missing

Table 5
Dipole Moment Components

Conformation	μ_a	μ_b	μ_c
D-in-plane	1.640	0.724	0.0
D-out-of-plane	1.628	0.751	0.008

Notes. Numerical values for the dipole moment components, in Debye, used in the line intensity calculation were retrieved from those of the normal species (Margulès et al. 2010).

Table 6
Partition Function Q_{rot} for Several Values of the Temperature T in Kelvin.

T/K	Q_{rot}	T/K	Q_{rot}	T/K	Q_{rot}	T/K	Q_{rot}
9.375	276	37.500	3619	150.000	34489	300.000	100582
18.750	1047	75.000	11474	225.000	64705		

Notes. In agreement with Coudert et al. (2012), the energy of the 0_{00} level of the D-in-plane conformation was taken equal to zero; that of the 0_{00}, + level of the D-out-of-plane conformation was assumed to be 10 cm^{-1}.

Table 7
Line List[a] for the Microwave Spectrum[b] of $HCOOCH_2D$

FREQ	ERR	LGINT	ELO	J'	K'_a	K'_c	±	J''	K''_a	K''_c	±
50041.7982	0.5000	−6.1442	44.1007	12	3	9	−	12	2	10	−
50044.2220	0.5000	−7.9394	143.9912	25	3	22	+	24	5	19	+
50046.6345	0.5000	−6.1442	44.0989	12	3	9	+	12	2	10	+
50046.6994	0.5000	−7.4039	232.0113	25	15	11	−	26	14	12	−
50046.6994	0.5000	−7.4039	232.0113	25	15	10	−	26	14	13	−
50053.4958	0.5000	−7.3976	232.0120	25	15	11	+	26	14	12	+
50053.4958	0.5000	−7.3976	232.0120	25	15	10	+	26	14	13	+
50070.5600	0.5000	−7.9389	143.9905	25	3	22	−	24	5	19	−
50071.4186	0.5000	−8.2617	98.7511	20	3	17	−	21	2	20	−
50078.3048	0.5000	−8.3046	207.2301	31	6	26		32	4	29	

Notes.
[a] Columns FREQ, ERR, LGINT, and ELO contain the line frequency in MHz, the error, also in MHz, the base 10 logarithm of the line intensity in $nm^2 \cdot MHz$ at 300 K, and the lower level energy (ELO) in cm^{-1}. The eight remaining columns contain the line assignment in terms of J, K_a, K_c, and the tunneling label ±. The latter is + or − for the two tunneling sublevels of the D-out-of-plane conformation and blank for the D-in-plane conformation.
[b] The line list is built using the results of the line-frequency analysis reported in this work.

(This table is available in its entirety in a machine-readable form in the online journal. A portion is shown here for guidance regarding its form and content.)

Table 8
Physical and Chemical Parameters Derived for Different Species

Parameter	$HCOOCH_2D$	$DCOOCH_3$	$HCOOCH_3$	^{13}C–$HCOOCH_3$ $v_t = 1$	CH_3CH_2OCOH	CH_3CH_2CN
d (″)	15	15	15	15	15	4–10
off (″)	7	7	7	7	7	5
T_{rot} (K)	110	110–250	110–250	110–250	150	110–275
Δv_{FWHM} (km s^{-1})	4	4	4	3	3	5–13
v_{LSR} (km s^{-1})	7.5	7.5	7.5	7	8	3–5
Component	Comp. ridge	Comp. ridge	Comp. ridge	Comp. ridge	Comp. ridge	Hot core
N_{comp} (cm^{-2})	5.0×10^{14}	5.0×10^{14}	1.2×10^{16}	6.6×10^{14}	4.5×10^{14}	3.8×10^{16}
N_{tot} (cm^{-2})	5.0×10^{14}	7.8×10^{14}	2×10^{16}	6.6×10^{14}	4.5×10^{14}	4.1×10^{16}

Notes. Parameters are compiled from Margulès et al. (2010), Tercero et al. (2013), Daly et al. (2013), and Haykal et al. (2013a). Column density values are given for each conformation, conformer, or state.

in the 168 GHz wide bandwidth covered. In order to model this emission, rotational constants of the D-out-of-plane conformation derived from this study, a fit to all the transitions of the D-in-plane conformation provided by Margulès et al. (2009a), and dipole moment from Curl (1959) have been implemented in the MADEX code (Cernicharo 2012). The D-in-plane conformation and the two tunneling substates of the D-out-of-plane conformation have been considered to be an independent molecular species for the calculation of line intensities. Owing to the lack of collisional rates for this molecule, the synthetic spectrum of these deuterated isotopologues of methyl formate was calculated assuming local thermodynamic equilibrium conditions. Only one component from this source (see, e.g., Blake et al. 1987; Schilke et al. 2001; Tercero et al. 2010 for Orion KL's components information), the compact ridge, has been necessary to properly model all lines arising from these species. We have adopted a size of 15″ and an offset 7″ from the pointing position (IRc2) of the compact ridge component (see, e.g., Favre et al. 2011). Beam dilution for each line has been taken into account in the calculation of the emerging line intensities. The physical/chemical parameters derived by the model are a kinetic temperature of 110 ± 20 K, a local standard of rest (LSR) velocity of the cloud of 7.5 km s^{-1}, a line width of 4 km s^{-1}, and a column density for each conformation of $(5.0 \pm 1.0) \times 10^{14}$ cm^{-2}.

In this paper, we simplify the models used in Margulès et al. 2010 and Tercero et al. 2012. In these previous papers, we used the cloud components detected and modeled for the strong methyl formate lines. However, all these contributions are difficult to distinguish in the weak lines of both conformations of $HCOOCH_2D$, as the contribution from the compact ridge is mainly responsible for the observed line profiles. Besides, in spite of the need to include several components of Orion KL to properly fit the line profiles of methyl formate, both the main species and the ^{13}C isotopologues, and vibrationally excited methyl formate (Haykal et al. 2013a), the compact ridge component also appears to be the main contribution to the emission. In Table 8, we compare several observed and derived physical and chemical parameters obtained for different species. We include the values of the calculated column density in the shown component and the total column density in all the components considered when we analyzed the emission of the corresponding species. For methyl formate and ^{13}C–$HCOOCH_3$ $v_t = 1$, a temperature gradient of the compact ridge is required for fitting all lines arising in our survey. The line profiles of $DCOOCH_3$ could probably be fit properly using a single rotational temperature. However, in Margulès et al. (2010), we used the same components that those obtained for $HCOOCH_3$ in order to assess the detection of the deuterated species. For ethyl formate (CH_3CH_2OCOH), a single rotational

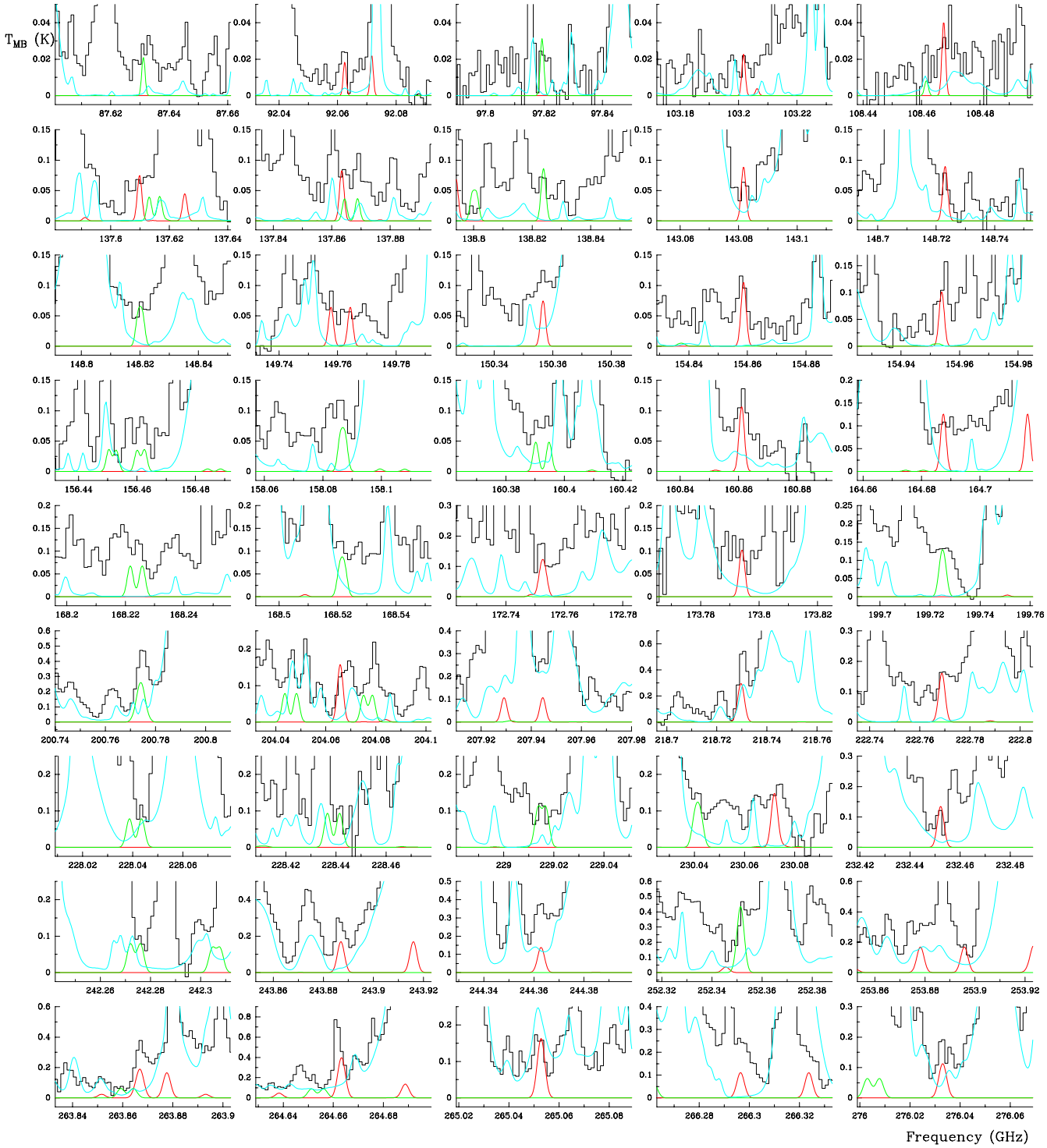

Figure 3. Selected lines of the D-out-of-plane (green) and D-in-plane (red) conformations of $HCOOCH_2D$ toward Orion-IRc2. The solid cyan line corresponds to all lines already modeled in our previous papers (see the text).

(A color version of this figure is available in the online journal.)

temperature (150 K) yields good fits between the data and a synthetic spectrum (Tercero et al. 2013). Finally, we included ethyl cyanide (CH_2CH_3CN; Daly et al. 2013) in Table 8 for contrasting the parameters obtained for molecules with high abundances in the compact ridge with one high-abundance molecule in the hot core.

We have obtained consistent results in all the works related to methyl formate. Both column density ratios, N(D-out-of-plane conformation)/$N(HCOOCH_3)$ and N(D-in-plane conformation)/$N(HCOOCH_3)$ (see Margulès et al. 2010 for column density results of methyl formate), give a value of 0.04 ± 0.02 for the compact ridge (taking into account both compact ridge components considered for $HCOOCH_3$), in agreement with that obtained for $N(DCOOCH_3)/N(HCOOCH_3)$ by Margulès et al. (2010), who derived 0.06 and 0.02 for the *hot* compact ridge and compact ridge, respectively. Similar abundance ratios have been found by different authors in the compact ridge component: $N(HDO)/N(H_2O) = 0.03$

Table 9
Detected Lines of $HCOOCH_2D$

J	K_a	K_c	±	J'	K'_a	K'_c	±	Predicted Freq. (MHz)	Error (MHz)	E_u (K)	S_{ij} (D^2)	Observed Freq. (MHz)	Obs. v_{LSR} (km s^{-1})	T_{mb}[a] (K)	Blend
8	0	8	−	7	0	7	−	87631.062	0.005	15.2	20.8	87631.0	7.7 ± 1.7	0.02	
8	0	8	+	7	0	7	+	87631.593	0.005	15.2	20.8	†	9.5 ± 1.7		
8	2	7		7	2	6		90089.776	0.002	22.3	19.8	90089.3	9.1 ± 1.7	0.02	
8	4	5		7	4	4		92062.615	0.002	30.7	15.9	92062.9	6.6 ± 1.6	0.03	
9	1	9	−	8	1	8	−	97329.436	0.006	20.0	23.4	97330.0	5.8 ± 1.5	0.05	
9	1	9	+	8	1	8	+	97329.987	0.006	20.0	23.4	†	7.5 ± 1.5		
9	0	9	−	8	0	8	−	97819.262	0.006	19.9	23.4	97819.0	8.3 ± 1.5	0.02	
9	0	9	+	8	0	8	+	97819.764	0.006	19.9	23.4	†	9.8 ± 1.5		
9	7	3		8	7	2		103201.885	0.002	58.1	9.46	103201.9	7.5 ± 1.5	0.02	
9	7	2		8	7	1		103201.886	0.002	58.1	9.46	†	7.5 ± 1.5		
9	6	4		8	6	3		103296.342	0.002	49.3	13.9	103296.0	8.5 ± 1.5	0.02	
9	6	3		8	6	2		103296.420	0.002	49.3	13.9	†	8.7 ± 1.5		
9	4	5		8	4	4		103857.559	0.002	35.7	19.2	103857.0	9.1 ± 1.4	0.03	
9	3	6		8	3	5		105527.227	0.002	31.1	21.3	105529.0	2.5 ± 1.4	0.06	$HCOOCH_3$ $v_t = 1$
9	3	7	−	8	3	6	−	107931.645	0.005	27.1	21.2	107933.5	2.3 ± 1.4	0.05	CH_3CH_2OCOH
9	3	7	+	8	3	6	+	107934.070	0.005	27.1	21.2	†	9.1 ± 1.4		
9	4	6	−	8	4	5	−	108317.278	0.008	31.3	18.9	108318.0	5.5 ± 1.4	0.04	
9	4	6	+	8	4	5	+	108318.144	0.006	31.3	19.1	†	7.9 ± 1.4		
9	2	7		8	2	6		108467.754	0.002	28.4	22.8	108468.0	6.8 ± 1.4	0.03	
9	4	5	−	8	4	4	−	108619.766	0.007	31.3	19.1	108620.9	4.4 ± 1.4	0.03	
9	4	5	+	8	4	4	+	108620.764	0.009	31.3	18.9	†	7.1 ± 1.4		
10	2	9		9	2	8		111650.695	0.002	32.5	25.4	111651.9	4.3 ± 1.3	0.06	
10	7	4		9	7	3		114734.301	0.002	63.6	13.6	114734.9	5.9 ± 1.3	0.09	CH_2CHCN $\nu_{15} = 1$
10	7	3		9	7	2		114734.304	0.002	63.6	13.6	†	5.9 ± 1.3		
10	6	5		9	6	4		114865.222	0.002	54.8	17.0	114866.9	3.1 ± 1.3	0.11	U
10	6	4		9	6	3		114865.513	0.002	54.8	17.0	†	3.9 ± 1.3		
11	0	11		10	0	10		114872.867	0.003	34.0	29.0	114871.9	10.0 ± 1.3	0.11	$HCOOCH_3$ $v_t = 2$
10	4	7		9	4	6		115395.477	0.002	41.2	22.3	115395.9	6.4 ± 1.3	0.12	CH_3CH_2OCOH
11	4	7	+	10	4	6	+	133953.756	0.005	43.5	25.3	133953.8	7.4 ± 1.1	0.07	
13	1	13		12	1	12		134638.258	0.003	46.5	34.3	134638.8	6.3 ± 1.1	0.25	CH_3CH_2CN ν_{13}/ν_{21}
12	1	11		11	1	10		135401.324	0.003	44.4	31.1	135398.0	14.9 ± 1.1	0.07	CH_3CHO $v_t = 1$
12	3	10		11	3	9		137610.084	0.003	49.1	29.8	137609.8	8.1 ± 1.1	0.07	
11	2	9	−	10	2	8	−	137613.363	0.005	37.7	28.1	137612.8	8.7 ± 1.1	0.07	$HCOOCH_3$
12	7	6		11	7	5		137863.652	0.003	76.3	21.0	137864.9	4.8 ± 1.1	0.08	
12	7	5		11	7	4		137863.709	0.003	76.3	21.0	†	4.9 ± 1.1		
11	3	8	−	10	3	7	−	137864.659	0.006	40.0	27.1	†	7.0 ± 1.1		
11	3	8	+	10	3	7	+	137869.082	0.005	40.0	27.1	137869.8	5.9 ± 1.1	0.11	U
13	1	13	−	12	1	12	−	138823.866	0.007	43.6	34.0	138823.9	7.4 ± 1.1	0.07	
13	1	13	+	12	1	12	+	138824.329	0.007	43.6	34.0	†	8.4 ± 1.1		
13	0	13	−	12	0	12	−	138883.386	0.007	43.6	34.0	138883.8	6.6 ± 1.1	0.23	U
13	0	13	+	12	0	12	+	138883.830	0.007	43.6	34.0	†	7.6 ± 1.1		
12	4	8		11	4	7		139847.915	0.003	54.1	28.4	139846.8	9.9 ± 1.1	0.07	CH_3COOCH_3
13	2	12		12	2	11		143081.943	0.003	51.6	33.5	143081.8	7.8 ± 1.0	0.06	
13	3	11		12	3	10		148723.308	0.003	56.3	32.7	148722.8	8.5 ± 1.0	0.07	
13	1	12	−	12	1	11	−	148819.613	0.006	48.7	33.3	148820.9	4.9 ± 1.0	0.07	
13	1	12	+	12	1	11	+	148821.114	0.006	48.7	33.3	†	7.9 ± 1.0		
14	1	14	−	13	1	13	−	149157.880	0.007	50.8	36.7	149158.1	7.1 ± 1.0	0.10	
14	1	14	+	13	1	13	+	149158.320	0.008	50.8	36.7	†	7.9 ± 1.0		
13	9	5		12	9	4		149158.892	0.003	105.2	18.0	†	9.1 ± 1.0		
13	9	4		12	9	3		149158.892	0.003	105.2	18.0	†	9.1 ± 1.0		
14	0	14	−	13	0	13	−	149191.398	0.007	50.8	36.7	149190.7	8.9 ± 1.0	0.43	$HCOOCH_3$ $(CH_3)_2CO$
14	0	14	+	13	0	13	+	149191.825	0.008	50.8	36.7	†	9.8 ± 1.0		
13	6	8		12	6	7		149758.006	0.003	74.7	27.1	149758.8	5.9 ± 1.0	0.10	
13	6	7		12	6	6		149764.600	0.003	74.7	27.1	149764.9	6.9 ± 1.0	0.06	
13	5	8		12	5	7		150356.939	0.003	67.3	29.5	150356.8	7.8 ± 1.0	0.12	
15	1	15		14	1	14		154678.384	0.004	60.8	39.6	154678.7	6.9 ± 1.0	0.17	$CH_3CH_2{}^{13}CN$
14	1	13		13	1	12		154858.948	0.003	58.8	36.1	154857.7	9.9 ± 1.0	0.12	CH_3OCH_3 $HCOOCH_3$
13	2	11		12	2	10		154954.147	0.003	54.8	33.5	154955.7	4.5 ± 1.0	0.15	U
13	8	6	+	12	8	5	+	155774.954	0.006	86.5	21.4	155775.7	6.1 ± 1.0	0.08	$CH_2{}^{13}CHCN$
13	8	5	+	12	8	4	+	155774.958	0.006	86.5	21.4	†	6.1 ± 1.0		
13	3	10		12	3	9		156388.308	0.003	57.5	32.7	156389.3	5.6 ± 1.0	0.07	
13	6	8	−	12	6	6	+	156460.298	0.020	69.8	25.9	156461.8	4.6 ± 1.0	0.07	
13	6	7	−	12	6	6	−	156462.818	0.009	69.8	26.9	†	9.5 ± 1.0		
14	2	13	−	13	2	12	−	158086.241	0.006	56.4	35.9	158086.2	7.6 ± 0.9	0.12	
14	2	13	+	13	2	12	+	158087.889	0.006	56.4	35.9	†	10.0 ± 0.9		
14	1	13	−	13	1	12	−	158894.305	0.006	56.3	35.9	158894.8	6.6 ± 0.9	0.11	
14	1	13	+	13	1	12	+	158895.777	0.006	56.3	35.9	†	9.3 ± 0.9		

Table 9
(Continued)

J	K_a	K_c	±	J'	K'_a	K'_c	±	Predicted Freq. (MHz)	Error (MHz)	E_u (K)	S_{ij} (D^2)	Observed Freq. (MHz)	Obs. v_{LSR} (km s^{-1})	T_{mb}[a] (K)	Blend
14	3	12		13	3	11		159698.558	0.003	63.9	35.3	159699.7	5.4 ± 0.9	0.08	
13	4	9	−	12	4	8	−	160390.473	0.006	58.3	31.2	160390.5	7.4 ± 0.9	0.08	
13	4	9	+	12	4	8	+	160395.030	0.005	58.3	31.2	160394.3	8.9 ± 0.9	0.08	
14	8	7		13	8	6		160861.326	0.003	101.4	25.1	160861.7	6.8 ± 0.9	0.13	$CH_2{}^{13}CHCN$
14	8	6		13	8	5		160861.337	0.003	101.4	25.1	†	6.8 ± 0.9		
15	1	14		14	1	13		164606.241	0.004	66.7	38.8	164605.7	8.5 ± 0.9	0.11	
16	1	16		15	1	15		164687.734	0.004	68.7	42.2	164688.7	5.7 ± 0.9	0.10	
14	4	10		13	4	9		164866.756	0.003	69.3	34.3	164866.7	7.6 ± 0.9	0.10	CH_3CH_2OCOH
14	8	7	−	13	8	6	−	167890.903	0.006	94.6	25.0	167889.7	9.6 ± 0.9	0.23	$(CH_3)_2CO$
14	8	6	−	13	8	5	−	167890.915	0.006	94.6	25.0	†	9.7 ± 0.9		
14	7	8	−	13	7	7	−	168221.588	0.006	85.6	27.8	168224.3	2.7 ± 0.9	0.12	$DCOOCH_3$
14	7	7	−	13	7	6	−	168222.376	0.006	85.6	27.8	†	4.1 ± 0.9		
14	7	8	+	13	7	7	+	168225.681	0.006	85.6	27.9	†	10.0 ± 0.9		
14	7	7	+	13	7	6	+	168226.470	0.006	85.6	27.8	†	11.4 ± 0.9		
15	2	14	−	14	2	13	−	168521.077	0.006	64.5	38.5	168521.8	6.2 ± 0.9	0.12	
15	2	14	+	14	2	13	+	168522.677	0.006	64.5	38.5	†	9.1 ± 0.9		
14	4	11	−	13	4	10	−	169016.309	0.005	66.0	34.0	169015.5	8.9 ± 0.9	0.20	U
15	1	14	−	14	1	13	−	169033.485	0.006	64.4	38.6	169035.6	3.7 ± 0.9	0.24	$HC^{18}OOCH_3$
15	1	14	+	14	1	13	+	169034.944	0.006	64.4	38.6	†	6.3 ± 0.9		
15	7	9		14	7	8		172752.270	0.003	99.5	31.1	172752.6	6.9 ± 0.9	0.17	
15	7	8		14	7	7		172753.589	0.003	99.5	31.7	†	9.2 ± 0.9		
15	5	11		14	5	10		173794.446	0.003	83.4	35.3	173794.7	7.1 ± 0.9	0.12	
18	1	17	−	17	1	16	−	199724.700	0.006	91.7	46.5	199727.6	3.1 ± 0.8	0.15	U
18	1	17	+	17	1	16	+	199726.122	0.006	91.7	46.5	†	5.3 ± 0.8		
16	3	14		15	2	13		199921.119	0.006	80.8	3.19	199921.4	7.1 ± 0.8	0.03	
19	1	19	−	18	1	18	−	200773.519	0.008	94.0	49.9	200775.2	5.0 ± 0.7	0.49	CH_3CH_2OH
19	1	19	+	18	1	18	+	200773.843	0.008	94.0	49.9	†	5.5 ± 0.7		
19	0	19	−	18	0	18	−	200775.163	0.008	94.0	49.9	†	7.4 ± 0.7		
19	0	19	+	18	0	18	+	200775.485	0.008	94.0	49.9	†	7.9 ± 0.7		
17	9	9	−	16	9	8	−	204043.999	0.006	132.4	32.5	204047.2	2.8 ± 0.7	0.14	$H^{13}COOCH_3$
17	9	8	−	16	9	7	−	204043.999	0.006	132.4	32.5	†	2.8 ± 0.7		
17	9	9	+	16	9	8	+	204048.616	0.006	132.4	32.5	†	9.6 ± 0.7		
17	9	8	+	16	9	7	+	204048.616	0.006	132.4	32.5	†	9.6 ± 0.7		
19	1	18		18	1	17		204066.071	0.004	103.1	49.4	204069.6	2.3 ± 0.7	0.16	$HCOO^{13}CH_3$
17	4	14	−	16	4	13	−	204075.369	0.005	93.8	42.4	204079.7	1.1 ± 0.7	0.20	$H^{13}CCCN$ $\nu_7 = 2$
17	4	14	+	16	4	13	+	204078.908	0.005	93.8	42.4	†	6.3 ± 0.7		
18	10	9		17	10	8		206850.006	0.003	162.2	33.2	206847.6	11.0 ± 0.7	0.15	CH_3CH_2CN ν_{13}/ν_{21}
18	10	8		17	10	7		206850.006	0.003	162.2	33.2	†	11.0 ± 0.7		
6	6	1	−	5	5	0	−	209621.621	0.013	29.5	3.01	209621.4	7.8 ± 0.7	0.15	$HCOOCH_3$ $\nu_t = 1$
6	6	0	−	5	5	1	−	209621.634	0.013	29.5	3.01	†	7.8 ± 0.7		
6	6	1	+	5	5	0	+	209622.126	0.013	29.5	3.11	†	8.5 ± 0.7		
6	6	0	+	5	5	−	+	209622.139	0.013	29.5	3.11	†	8.6 ± 0.7		
17	5	12	−	16	5	11	−	209716.882	0.006	99.7	41.2	209718.9	4.6 ± 0.7	0.22	$H^{13}COOCH_3$
17	5	12	+	16	5	11	+	209722.127	0.006	99.7	41.2	†	12.1 ± 0.7		
19	1	18	−	18	1	17	−	210004.925	0.006	101.8	49.1	210005.0	7.4 ± 0.7	0.53	$(CH_3)_2CO$
19	1	18	+	18	1	17	+	210006.329	0.006	101.8	49.1	†	9.4 ± 0.7		
20	1	20	−	19	1	19	−	211091.566	0.008	104.2	52.6	211096.3	0.8 ± 0.7	0.45	CH_3OH
20	1	20	+	19	1	19	+	211091.865	0.009	104.2	52.6	†	1.2 ± 0.7		
20	0	20	−	19	0	19	−	211092.448	0.008	104.2	52.6	†	2.0 ± 0.7		
20	0	20	+	19	0	19	+	211092.747	0.009	104.2	52.6	†	2.5 ± 0.7		
18	5	13		17	5	12		211553.756	0.004	112.1	44.1	211552.5	9.3 ± 0.7	0.10	
19	3	17		18	3	16		212534.733	0.004	109.9	48.9	212536.2	5.4 ± 0.7	0.18	
20	2	19		19	2	18		213887.260	0.004	113.3	52.1	213885.0	10.7 ± 0.7	0.26	$^{13}CH_3CH_2CN$ CH_2CHCN $\nu_{11} = 2$
18	4	14		17	4	13		216782.819	0.004	107.2	45.7	216782.5	7.9 ± 0.7	0.38	$(CH_3)_2CO$
19	9	11		18	9	10		218729.508	0.003	159.8	39.1	218731.2	5.2 ± 0.7	0.58	CH_2CHCN $\nu_{15} = 1$
19	9	10		18	9	9		218729.557	0.003	159.8	39.1	†	5.2 ± 0.7		
19	4	16		18	4	15		218730.506	0.004	116.1	48.1	†	6.5 ± 0.7		
20	1	19	−	19	1	18	−	220296.238	0.006	112.4	51.8	220297.5	5.8 ± 0.7	0.39	$CH_3{}^{13}CN$
20	1	19	+	19	1	18	+	220297.622	0.006	112.4	51.8	†	7.7 ± 0.7		
7	6	2	−	6	5	1	−	221560.202	0.012	33.5	3.01	221560.0	7.8 ± 0.7	0.07	
7	6	1	−	6	5	2	−	221560.342	0.012	33.5	3.01	†	8.0 ± 0.7		
7	6	2	+	6	5	1	+	221561.002	0.013	33.5	3.11	†	8.9 ± 0.7		
7	6	1	+	6	5	2	+	221561.142	0.013	33.5	3.11	†	9.0 ± 0.7		
20	3	18		19	3	17		222769.101	0.004	120.6	51.5	222770.0	6.3 ± 0.7	0.17	
22	1	22		21	1	21		224689.136	0.005	126.3	58.2	224690.0	6.3 ± 0.7	0.31	
22	0	22		21	0	21		224690.264	0.005	126.3	58.2	†	7.9 ± 0.7		
19	9	11	−	18	9	9	+	228441.909	0.006	153.7	39.1	228442.4	6.9 ± 0.7	0.11	
19	9	11	+	18	9	10	+	228441.928	0.006	153.7	39.1	†	6.9 ± 0.7		

Table 9
(Continued)

J	K_a	K_c	±	J'	K'_a	K'_c	±	Predicted Freq. (MHz)	Error (MHz)	E_u (K)	S_{ij} (D^2)	Observed Freq. (MHz)	Obs. v_{LSR} (km s^{-1})	T_{mb}[a] (K)	Blend
19	8	11	+	18	8	11	−	229013.808	0.011	143.6	40.8	229015.1	5.8 ± 0.7	0.12	
19	8	11	−	18	8	10	−	229014.351	0.008	143.6	41.2	†	6.5 ± 0.7		
19	8	12	+	18	8	11	+	229016.905	0.008	143.6	41.2	†	9.9 ± 0.7		
19	8	12	−	18	8	10	+	229017.452	0.011	143.6	40.8	†	10.6 ± 0.7		
19	4	15		18	4	14		229518.326	0.004	118.2	48.4	229519.3	6.2 ± 0.7	0.14	
20	11	10		19	11	9		229839.213	0.004	198.0	37.2	229837.5	9.7 ± 0.7	0.37	
20	11	9		19	11	8		229839.213	0.004	198.0	37.2	†	9.7 ± 0.7		
19	7	13	−	18	7	12	−	229841.076	0.008	134.8	43.1	†	12.2 ± 0.7		
19	7	13	+	18	7	12	+	229843.578	0.008	134.8	43.3	†	15.4 ± 0.7		
19	7	12	−	18	7	11	−	229964.664	0.008	134.8	43.3	229966.1	5.6 ± 0.7	0.22	CH_2CHCN $\nu_{11} = 3$
19	7	12	+	18	7	11	+	229967.228	0.009	134.8	43.1	†	9.0 ± 0.7		
20	2	18	−	19	2	17	−	230040.745	0.006	119.7	51.1	230042.4	5.3 ± 0.7	0.15	
20	2	18	+	19	2	17	+	230042.772	0.006	119.7	51.1	†	8.0 ± 0.7		
20	10	11		19	10	10		230072.391	0.003	183.8	39.9	230071.1	9.2 ± 0.7	0.15	
20	10	10		19	10	9		230072.394	0.003	183.8	39.9	†	9.2 ± 0.7		
20	9	12		19	9	11		230398.724	0.003	170.9	42.5	230397.4	9.2 ± 0.7	0.27	CH_2CHCN $\nu_{15} = 1$
20	9	11		19	9	10		230398.847	0.003	170.9	42.5	†	9.4 ± 0.7		
19	6	14	−	18	6	13	−	230761.120	0.006	127.3	45.4	230766.2	0.9 ± 0.7	0.22	U
19	6	14	+	18	6	13	+	230764.944	0.006	127.3	45.4	†	5.9 ± 0.7		
20	8	13		19	8	12		230870.631	0.003	159.4	44.6	230868.7	10.0 ± 0.6	0.40	$CH_2{}^{13}CHCN$
20	8	12		19	8	11		230873.895	0.003	159.4	44.6	†	14.3 ± 0.6		
20	7	14		19	7	13		231568.004	0.004	149.4	46.8	231569.8	5.2 ± 0.6	0.12	
20	6	15		19	6	14		232452.669	0.004	140.8	48.4	232452.4	7.8 ± 0.6	0.12	
20	5	16		19	5	15		232572.679	0.004	133.6	49.7	232573.9	5.9 ± 0.6	0.23	$CH_3{}^{13}CH_2CN$
21	2	19		20	2	18		234054.276	0.004	131.7	54.2	234054.3	7.5 ± 0.6	0.31	
20	3	17		19	3	16		236549.822	0.004	126.0	51.5	236547.7	10.2 ± 0.6	0.31	$DCOOCH_3$
21	3	19	−	20	3	18	−	239765.256	0.005	131.3	53.7	239766.3	6.2 ± 0.6	0.27	
21	3	19	+	20	3	18	+	239767.464	0.006	131.3	53.7	239768.3	6.5 ± 0.6	0.26	
20	5	16	+	19	5	15	+	242276.461	0.006	132.5	49.6	242276.4	7.6 ± 0.6	0.10	
23	2	22		22	2	21		243887.433	0.005	147.0	60.0	243886.3	8.9 ± 0.6	0.30	^{34}SHD
21	6	16		20	6	15		244363.298	0.004	152.5	51.3	244363.4	7.4 ± 0.6	0.38	
24	0	24		23	1	23		244678.199	0.005	149.3	10.3	244680.3	4.9 ± 0.6	0.44	U
24	1	24		23	1	23		244678.682	0.005	149.3	63.5	†	5.5 ± 0.6		
24	0	24		23	0	23		244679.051	0.005	149.3	63.5	†	6.0 ± 0.6		
24	1	24		23	0	23		244679.534	0.005	149.3	10.3	†	6.6 ± 0.6		
22	3	20	−	21	3	19	−	250108.540	0.006	143.3	56.4	250111.3	4.2 ± 0.6	0.22	U
22	3	20	+	21	3	19	+	250110.680	0.006	143.3	56.4	†	6.8 ± 0.6		
24	0	24	−	23	1	23	−	252351.616	0.010	149.6	12.7	252352.6	6.3 ± 0.6	0.48	
24	1	24	−	23	1	23	−	252351.693	0.010	149.6	63.2	†	6.4 ± 0.6		
24	0	24	−	23	0	23	−	252351.763	0.010	149.6	63.2	†	6.5 ± 0.6		
24	0	24	+	23	1	23	+	252351.810	0.010	149.6	12.7	†	6.6 ± 0.6		
24	1	24	−	23	0	23	−	252351.840	0.010	149.6	12.7	†	6.6 ± 0.6		
24	1	24	+	23	1	23	+	252351.888	0.010	149.6	63.2	†	6.7 ± 0.6		
24	0	24	+	23	0	23	+	252351.958	0.010	149.6	63.2	†	6.7 ± 0.6		
24	1	24	+	23	0	23	+	252352.035	0.010	149.6	12.7	†	6.8 ± 0.6		
24	2	23		23	2	22		253878.590	0.005	159.2	62.7	253878.2	8.0 ± 0.6	0.31	$CH_3CH_2{}^{13}CN$
24	1	23		23	1	22		253896.118	0.005	159.2	62.7	253896.3	7.3 ± 0.6	0.19	
22	8	15		21	8	14		254451.934	0.004	183.3	50.7	254455.0	3.9 ± 0.6	0.27	$H^{13}COOCH_3$ $v_t = 1$
22	8	14		21	8	13		254465.903	0.004	183.3	50.7	254466.3	7.0 ± 0.6	0.28	U
22	12	11	+	21	12	10	+	263859.673	0.007	227.7	41.0	263860.3	6.8 ± 0.6	0.04	
22	12	10	+	21	12	9	+	263859.673	0.007	227.7	41.0	†	6.8 ± 0.6		
22	12	11	−	21	12	10	−	263864.631	0.007	227.7	41.0	263867.2	4.6 ± 0.6	0.39	
22	12	10	−	21	12	9	−	263864.631	0.007	227.7	41.0	†	4.6 ± 0.6		
23	16	8		22	16	7		263865.858	0.005	326.0	31.6	†	6.0 ± 0.6		
23	16	7		22	16	6		263865.858	0.005	326.0	31.6	†	6.0 ± 0.6		
25	2	24		24	2	23		263867.437	0.005	171.9	65.4	†	7.8 ± 0.6		
22	5	17		21	5	16		264078.565	0.004	159.0	55.5	264078.8	7.2 ± 0.6	0.18	CH_2DCH_2CN
7	7	1		6	6	0		264638.757	0.008	48.8	2.99	264639.2	7.0 ± 0.6	0.11	
7	7	0		6	6	1		264638.758	0.008	48.8	2.99	†	7.0 ± 0.6		
26	0	26		25	1	25		264663.455	0.006	174.2	11.2	264662.1	9.0 ± 0.6	0.79	CH_3CH_2OH $CH_2{}^{13}CHCN$
26	1	26		25	1	25		264663.609	0.006	174.2	68.8	†	9.2 ± 0.6		
26	0	26		25	0	25		264663.728	0.006	174.2	68.8	†	9.3 ± 0.6		
26	1	26		25	0	25		264663.883	0.006	174.2	11.2	†	9.5 ± 0.6		
23	10	14		22	10	13		265053.256	0.004	220.2	49.7	265053.8	6.9 ± 0.6	0.16	
23	10	13		22	10	12		265053.313	0.004	220.2	49.7	†	6.9 ± 0.6		
21	5	16	+	20	5	15	+	265136.706	0.008	146.6	52.8	265136.3	8.0 ± 0.6	0.13	
22	8	15	−	21	8	14	−	266193.006	0.009	180.2	49.9	266197.5	2.4 ± 0.6	0.15	CH_3OH
22	8	15	+	21	8	14	+	266195.626	0.010	180.2	49.9	†	5.4 ± 0.6		

Table 9
(Continued)

J	K_a	K_c	±	J'	K'_a	K'_c	±	Predicted Freq. (MHz)	Error (MHz)	E_u (K)	S_{ij} (D^2)	Observed Freq. (MHz)	Obs. v_{LSR} (km s^{-1})	T_{mb}[a] (K)	Blend
23	8	16		22	8	15		266296.865	0.004	196.1	53.7	266296.3	8.1 ± 0.6	0.26	
24	2	22	−	23	2	21	−	270832.373	0.006	168.8	61.6	270834.2	5.5 ± 0.6	0.15	
24	2	22	+	23	2	21	+	270834.338	0.006	168.8	61.6	†	7.7 ± 0.6		
25	1	24	−	24	2	23	−	271802.831	0.007	172.7	11.6	271807.1	2.8 ± 0.6	0.31	
25	1	24	+	24	2	23	+	271804.105	0.007	172.7	11.6	†	4.2 ± 0.6		
25	2	24	−	24	2	23	−	271805.499	0.007	172.7	65.0	†	5.7 ± 0.6		
25	2	24	+	24	2	23	+	271806.769	0.007	172.7	65.0	†	7.1 ± 0.6		
25	1	24	−	24	1	23	−	271807.685	0.007	172.7	65.0	†	8.1 ± 0.6		
25	1	24	+	24	1	23	+	271808.953	0.007	172.7	65.0	†	9.5 ± 0.6		
25	2	24	−	24	1	23	−	271810.352	0.007	172.7	11.6	†	11.1 ± 0.6		
25	2	24	+	24	1	23	+	271811.618	0.007	172.7	11.6	†	12.5 ± 0.6		
24	4	21		23	4	20		271820.670	0.004	176.3	61.4	271822.1	5.9 ± 0.6	0.26	CH_3CHO
26	0	26	−	25	1	25	−	272973.976	0.011	175.3	13.8	272974.1	7.4 ± 0.5	0.30	$DCOOCH_3$
26	1	26	−	25	1	25	−	272973.997	0.011	175.3	68.5	†	7.4 ± 0.5		
26	0	26	−	25	0	25	−	272974.017	0.011	175.3	68.5	†	7.4 ± 0.5		
26	1	26	−	25	0	25	−	272974.038	0.011	175.3	13.8	†	7.4 ± 0.5		
26	0	26	+	25	1	25	+	272974.116	0.011	175.3	13.8	†	7.5 ± 0.5		
26	1	26	+	25	1	25	+	272974.137	0.011	175.3	68.5	†	7.5 ± 0.5		
26	0	26	+	25	0	25	+	272974.156	0.011	175.3	68.5	†	7.6 ± 0.5		
26	1	26	+	25	0	25	+	272974.177	0.011	175.3	13.8	†	7.6 ± 0.5		
24	14	11		23	14	10		275628.745	0.005	298.5	42.0	275629.1	7.1 ± 0.5	0.22	
24	14	10		23	14	9		275628.745	0.005	298.5	42.0	†	7.1 ± 0.5		
24	12	13		23	12	12		276033.561	0.004	263.2	47.8	276033.6	7.5 ± 0.5	0.20	
24	12	12		23	12	11		276033.561	0.004	263.2	47.8	†	7.5 ± 0.5		

Notes. Emission lines of $HCOOCH_2D$ present in the spectral scan of Orion KL from the IRAM 30 m radio telescope. Columns 1–8 give the line assignment. + or − in Columns 4 and 8 identify the two tunneling sublevels of the D-out-of-plane conformation; a blank entry indicates a transition of the D-in-plane conformation. Column 9 gives the predicted frequency in the laboratory. Column 10 gives the uncertainty of frequency predictions. Column 11 is the upper level energy. Column 12 is the line strength. Column 13 is the observed frequency assuming a v_{LSR} of 7.5 km s^{-1}. Column 14 is the observed radial velocity, Column 15 the main beam temperature, and Column 16 gives blends. A † in Column 13 means that line is blended with a previous line.

[a] This value has to be considered an upper limit.

and $N(\mathrm{HDCO})/N(\mathrm{H_2CO}) = 0.01$ by Persson et al. (2007), $N(\mathrm{DCN})/N(\mathrm{HCN}) = 0.01$–$0.06$ by Schilke et al. (1992), and $N(\mathrm{HDCS})/N(\mathrm{H_2CS}) = 0.040 \pm 0.012$ by Tercero et al. (2010).

The full census of detected lines is provided in Table 9, where we list 66 unblended lines as well as 56 lines moderately blended with other species. Owing to the weakness of these features, the main bean antenna temperature and the radial velocity have been obtained from the peak channel of our spectra. Therefore, errors in the baselines and contribution from other species could affect the T_{mb} value, which has to be considered to be the total intensity of the detected feature and an upper limit on the intensity of deuterated methyl formate in this study. The uncertainty in the radial velocity has been adopted from the spectral resolution of our data. Line widths are not included in Table 9 due to the difficulty of obtaining this parameter from the data (overlap problems and/or weak lines). This identification is based on a whole inspection of the data and the modeled synthetic spectrum of the studied species and all the species already identified in our previous papers (see above). We consider blended lines to be those that are close enough to other stronger features. No missing lines were found in unblended frequencies of the spectra.

Rotational diagrams were included in order to judge the quality of the detection. The following equation relates the molecular parameters with the observed ones (see, e.g., Turner 1991; Goldsmith & Langer 1999; Persson et al. 2007 for a detailed discussion of the derivation):

$$\ln\left(\frac{N_u}{g_u}\right) = \ln\left(\frac{8\pi k \nu^2 W}{hc^3 A_{\mathrm{ul}} g_u b}\right) = \ln\left(\frac{N}{Q_{\mathrm{rot}}}\right) - \frac{E_{\mathrm{upp}}}{kT_{\mathrm{rot}}}, \quad (2)$$

where N_u is the column density in the upper state ($\mathrm{cm^{-2}}$), g_u is the statistical weight in the upper level, W (K cm s^{-1}) is the integrated line intensity (in main beam temperature), A_{ul} is the Einstein A-coefficient of spontaneous emission, N ($\mathrm{cm^{-2}}$) is the total column density, Q_{rot} is the rotational partition function, E_{upp} (K) is the upper level energy, T_{rot} (K) is the rotational temperature, and b is the beam dilution factor.

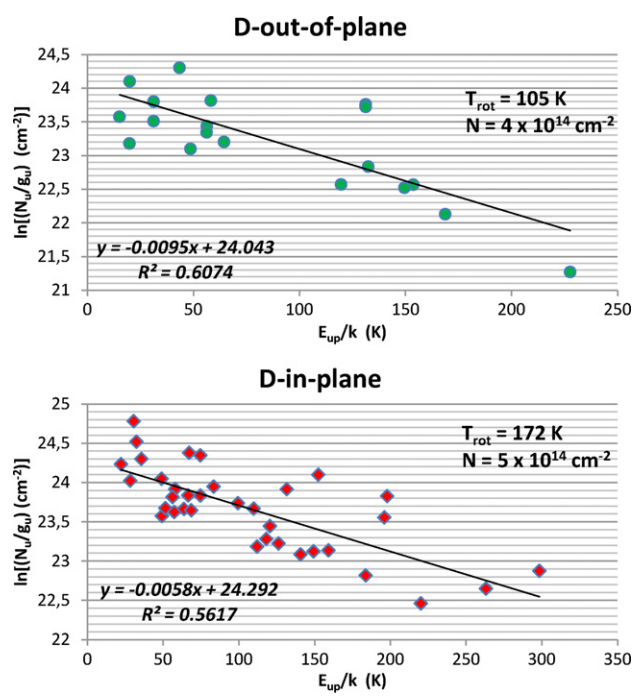

Figure 4. Rotational diagrams for both conformations of $HCOOCH_2D$.
(A color version of this figure is available in the online journal.)

The upper state column densities divided by the statistical weight are plotted as a function of the upper level energies for both conformations of $HCOOCH_2D$ in Figure 4, setting the line width to 4 km s^{-1}. The rotational temperature and the total column density can be derived from these plots by performing a linear least squares fit to the points. For the out-of-plane conformation, we used 20 transitions with upper level energies ranging from 15.2 to 227.7 K, while for the in-plane conformation we considered 35 transitions with energies between 22.3–298.5 K. We derived the rotational temperatures and column densities, $T_{rot} = 105 \pm 50$ K and $N = (4 \pm 2) \times 10^{14}$ cm^{-2} and $T_{rot} = 172 \pm 70$ K and $N = (5 \pm 2) \times 10^{14}$ cm^{-2}, for the out-of-plane and in-plane conformations, respectively. These results are in agreement with the values obtained in our model (see above), confirming the detection of $HCOOCH_2D$.

6. CONCLUSIONS

The pure rotational spectrum of $HCOOCH_2D$ was recorded in the laboratory from 0.77 to 1.2 THz. 1650 lines were assigned to the D-in-plane and D-out-of-plane conformations. A line-frequency analysis of the present dataset and of previously published transitions (Margulès et al. 2009a) was performed accounting for the large-amplitude torsional motion of the partially deuterated CH_2D methyl group taking place in the D-out-of-plane conformation. The experimental frequencies were reproduced with an rms of 0.16 MHz and the spectroscopic constants thus obtained are given in Tables 3 and 4. The line list built using the results of this analysis allowed us to detect $HCOOCH_2D$ in Orion KL. 66 unblended lines, as well as 56 lines that were moderately blended with other species, could be observed from both conformations. These detections, the good agreement between model and observations, and the consistent results between model and rotational diagrams ensure the detection of both conformations of $HCOOCH_2D$ in Orion. In addition, the observed deuteration enhancement is consistent with that obtained for other species in this source.

Portions of this paper present research carried out at the Jet Propulsion Laboratory, California Institute of Technology, under contract with the National Aeronautics and Space Administration. Government sponsorship is acknowledged. This work was also supported by the French program Action sur Projets de l'INSU "Physique et Chimie du Milieu Interstellaire" (PCMI) and by the contracts ANR-08-BLAN-0054 and ANR-08-BLAN-0225. J.C. and B.T. thank the Spanish MINECO for funding support from grants CSD2009-00038, AYA2009-07304, and AYA2012-32032.

REFERENCES

Bauder, A. 1979, JPCRD, 8, 583
Bell, T. A., Cernicharo, J., Viti, S., et al. 2013, A&A, submitted
Blake, G. A., Sutton, E. C., Masson, G. R., & Philips, T. G. 1986, ApJS, 60, 357
Blake, G. A., Sutton, E. C., Masson, C. R., & Phillips, T. G. 1987, ApJ, 315, 621
Brown, R. D., Crofts, J. G., Godfrey, P. D., et al. 1975, ApJL, 197, L29
Carvajal, M., Margulès, L., Tercero, B., et al. 2009, A&A, 500, 1109
Carvajal, M., Willaert, F., Demaison, J., & Kleiner, I. 2007, JMoSp, 246, 158
Cernicharo, J. 1985, Internal IRAM Report (Granada: IRAM)
Cernicharo, J. 2012, in ECLA-2011: Proc. of the European Conf. on Laboratory Astrophysics, EAS Publication Series, 2012, ed. C. Stehl, C. Joblin, & L. d'Hendecourt (Cambridge: Cambridge Univ. Press), 251
Coudert, L. H., Margulès, L., Huet, T. R., et al. 2012, A&A, 543, A46
Curl, R. F. 1959, JChPh, 30, 1529
Daly, A. M., Bermúdez, C., López, A., et al. 2013, ApJ, 768, 81
Demaison, J., Boucher, D., Dubrulle, A., & van Eijck, B. P. 1983, JMoSp, 102, 260
Demaison, J., Margulès, L., Kleiner, I., & Császár, A. G. 2010, JMoSp, 259, 70
Demyk, K., Bottinelli, S., Caux, E., et al. 2010, A&A, 517, A17
Demyk, K., Mäder, H., Tercero, B., et al. 2007, A&A, 466, 255
Demyk, K., Wlodarczak, G., & Carvajal, M. 2008, A&A, 489, 589
Drouin, B. J., Maiwald, F. W., & Pearson, J. C. 2005, RScI, 76, 093113
Esplugues, G. B., Cernicharo, J., Viti, S., et al. 2013b, A&A, 559, 51
Esplugues, G. B., Tercero, B., Cernicharo, J., et al. 2013a, A&A, 556, 143
Favre, C., Despois, D., Brouillet, N., et al. 2011, A&A, 532, A32
Goldsmith, P. F., & Langer, W. D. 1999, ApJ, 517, 209
Haykal, I., Carvajal, M., Tercero, B., et al. 2013a, A&A, submitted
Haykal, I., Margules, L., Huet, T. R., et al. 2013b, ApJ, 777, 120
Herbst, E. 1992, in Isotope Effects in Gas Phase Chemistry, ed. J. A. Kaye (Washington, DC: American Chemical Society), 358
Ilyushin, V., Kryvda, A., & Alekseev, E. 2009, JMoSp, 255, 32
Karakawa, Y., Oka, K., Odashima, H., Takagi, K., & Tsunekawa, S. 2001, JMoSp, 210, 196
Kobayashi, K., Ogata, K., Tsunekawa, S., & Takano, S. 2007, ApJL, 657, L17
Kolesniková, L., Daly, A. M., Alonso, J. L., Tercero, B., & Cernicharo, J. 2013, JMoSp, 289, 13
Margulès, L., Coudert, L. H., Møllendal, H., et al. 2009a, JMoSp, 254, 55
Margulès, L., Huet, T. R., Demaison, J., et al. 2010, ApJ, 714, 1120
Margulès, L., Motiyenko, R., Demyk, K., et al. 2009b, A&A, 493, 565
Motiyenko, R. A., Tercero, B., Cernicharo, J., & Margulès, L. 2012, A&A, 548, A71
Nummelin, A., Bergman, P., Hjalmarson, A., et al. 2000, ApJS, 128, 213
Oesterling, L. C., Albert, S., De Lucia, F. C., Sastry, K. V. L. N., & Herbst, E. 1999, ApJ, 521, 255
Ogata, K., Odashima, H., Takagi, K., & Tsunekawa, S. 2004, JMoSp, 225, 14
Pardo, J. R., Cernicharo, J., & Serabyn, E. 2001, ITAP, 49, 1683
Persson, C. M., Olofsson, A. O. H., Koning, N., et al. 2007, A&A, 476, 807
Pickett, H. M., Poynter, R. L., Cohen, E. A., et al. 1998, JQSRT, 60, 883
Plummer, G. M., Herbst, E., De Lucia, F. C., & Blake, G. A. 1984, ApJS, 55, 633
Plummer, G. M., Herbst, E., De Lucia, F. C., & Blake, G. A. 1986, ApJS, 60, 949
Schilke, P., Benford, D. J., Hunter, T. R., Lis, D. C., & Phillips, T. G. 2001, ApJS, 132, 281
Schilke, P., Walmsley, C. M., Pineau Des Forets, G., et al. 1992, A&A, 256, 595
Tercero, B., Cernicharo, J., Pardo, J. R., & Goicoechea, J. R. 2010, A&A, 517, A96
Tercero, B., Kleiner, I., Cernicharo, J., et al. 2013, ApJL, 770, L13
Tercero, B., Margulès, L., Carvajal, M., et al. 2012, A&A, 538, A119
Tercero, B., Vincent, L., Cernicharo, J., Viti, S., & Marcelino, N. 2011, A&A, 528, A26
Tudorie, M., Coudert, L. H., Huet, T. R., Jegouso, D., & Sedes, G. 2011, JChPh, 134, 074314
Turner, B. E. 1991, ApJS, 76, 617